Estimating Entire Geometric Parameter Errors of Manipulator Arm Using Laser Module and Stationary Camera

In-Won Park and Jong-Hwan Kim

Abstract— **This paper proposes a novel kinematic calibration technique to estimate entire geometric parameter errors of robot manipulator. There always exist small errors in link length and link twist for physical manipulators. These errors eventually affect the precision in kinematic equations, and cause inverse kinematic equations to calculate joint angle values having errors. In order to solve these problems, the proposed kinematic calibration technique employs a laser module and a stationary camera. The laser module made with three laser sources is attached to the end-effector of manipulator arm and the stationary camera is used to determine an accurate position of three laser beams on a 2D screen. A non-singular Jacobian matrix is formulated by using differential kinematics and transformation mapping equations to represent the variances between actual and measured positions of laser beams. Then two parameter estimation algorithms, least squares estimation and extended Kalman filter, are used to estimate the entire geometric parameter errors. Effectiveness of the proposed calibration technique is verified with 7 degrees of freedom MyBot humanoid arm by computer simulation.**

I. Introduction

All robot manipulators require a kinematic calibration to move the end-effector in a specified direction at a specified speed with accuracy. The most common sources of manipulator error are geometric and non-geometric errors. The geometric errors are mainly caused by an inaccurate knowledge of kinematic model such as errors existing in the nominal value of Denavit-Hartenberg (D-H) parameters. The non-geometric errors are generally caused by joint and link compliances, gear backlash, thermal, wear, etc. These errors must be determined and taken into the theoretical model because they eventually affect the precision in kinematic equations and cause the inverse kinematic equations to calculate joint angle values having errors.

To cope with the problem, many researches related to the manipulator calibration have been proposed [1]-[4]. In order to predict the geometric parameter errors, both position and orientation of the end-effector have to be measured. Omodei et al. [5] and Alici et al. [6] introduced a methodology that uses an optical system as the measuring device. Renaud et al. used a vision-based measuring device for the kinematic calibration of parallel mechanisms [7]. In addition, a pose-matching technique was demonstrated for measuring arm to provide a low-cost and easy-to-use external metrology system [8]-[10]. When the position information was only considered, it required a large number of measurements because the accuracy has been improved only in the measured positions. To overcome this problem, Iurascu et al. [11] and Ye et al. [12] presented a kinematic calibration method using differential kinematics.

Authors are with the Department of Electrical Engineering, KAIST, 335 Gwahak-ro (373-1 Guseong-dong), Yuseong-gu, Daejeon, 305-701, Republic of Korea, e-mail: ({iwpark, johkim}@rit.kaist.ac.kr).

This paper proposes a novel kinematic calibration technique to estimate entire geometric parameter errors of manipulator arm including the position and orientation of end-effector. A laser module made with three laser sources and a stationary camera are employed as the measuring device. The laser module is attached to the end-effector and the stationary camera is used to measure the positions of three laser beams on a 2D screen.

Due to the presence of geometric parameter errors, there exists a distance error between the measured position of laser beam on the screen and the theoretical position calculated from the kinematic equations. In order to estimate these parameter errors, this paper derives a non-singular Jacobian matrix that represents how each parameter error influences the variances between the measured and theoretical positions of laser beams. Differential kinematics and general transformation mapping equations are used to formulate this Jacobian matrix. Least squares estimation (LSE) and extended Kalman filter (EKF) are used as the parameter optimization algorithm and then their results are compared to each other.

The proposed kinematic calibration technique is verified with 7 degrees of freedom (DOF) MyBot humanoid arm in simulation. Simulation results confirm that the proposed technique completely estimates individual geometric parameter errors and simultaneously minimizes the distance error between the measured and the theoretical positions of laser beams on the screen. Since the proposed technique considers not only the location of end-effector, but also the velocity at which the end-effector moves, it requires a small number of measurements to estimate errors existing in the entire geometric parameters.

This paper is organized as follows: Section II describes the MyBot arm including laser module and its kinematics. Section III formulates the non-singular Jacobian matrix, which represents the relationship between entire geometric parameter errors and the positions of laser beams. Section IV explains LSE and EKF, which are used as the optimization algorithms to estimate the geometric parameter errors. Section V presents the simulation results of MyBot arm and concluding remarks follow in Section VI.

II. Proposed Kinematic Calibration System

The proposed kinematic calibration system is shown in Fig. 1, which consists of a manipulator arm, a laser module,

978-1-61284-972-0/11/$26.00 ©2011 IEEE

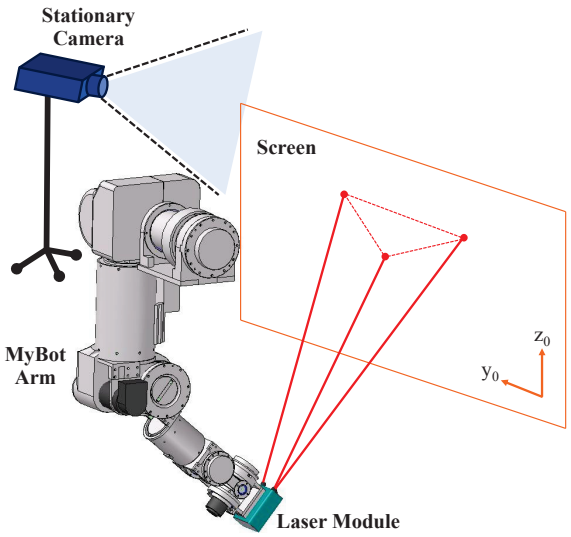

Fig. 1. Proposed kinematic calibration system.

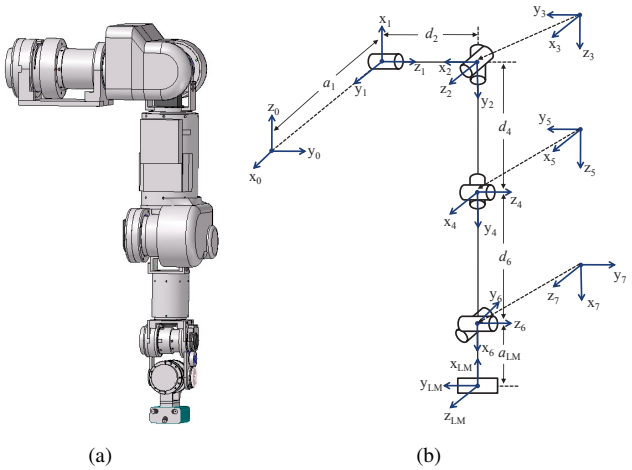

Fig. 2. MyBot arm. (a) Snapshot of MyBot arm having laser module. (b) D-H parameters and frame assignments of MyBot arm.

TABLE I
NOMINAL VALUES OF D-H PARAMETER FOR MYBOT ARM.

Joint	a_i (m)	d_i (m)	α_i (°)	β_i (°)	θ_i (°)	q_i (°)
1	-1.0	0.0	-90.0	0.0	-90.0	-180.0 ∽ 90.0
2	0.0	0.1	-90.0	N/A	90.0	-10.0 ∽ 90.0
3	0.0	0.0	-90.0	N/A	-90.0	-10.0 ∽ 30.0
4	0.0	0.2	90.0	N/A	0.0	-120.0 ∽ 0.0
5	0.0	0.0	-90.0	N/A	0.0	-90.0 ∽ 90.0
6	0.0	0.2	90.0	N/A	90.0	-30.0 ∽ 30.0
7	0.0	0.0	90.0	N/A	0.0	-30.0 ∽ 30.0
LM	0.05	0.0	0.0	0.0	180.0	0.0

a stationary camera, and a 2D screen. The laser module acts as a sensing device, which is attached to the end-effector of manipulator arm. The stationary camera measures the positions of laser beams on the 2D screen, which are beamed from the laser module. If the geometric parameters of manipulator arm are calibrated thoroughly, the theoretical position of laser beams calculated from the kinematic equations and the measured position of laser beams obtained from the stationary camera should be identical. However, there always exist small errors due to inaccurate knowledge of kinematic model. Thus, the main objective of this paper is to estimate all errors existing in the geometric parameters of manipulator arm to minimize the distance error between the theoretical and the measured positions of laser beams on the 2D screen.

The simulation model of MyBot arm having 7 DOF is used in the present work, which consists of 7 DC motors with harmonic drives to provide control accuracy, gear reduction, and sufficient power. It is mechanically designed such that four strain gauges will be attached on the surface of each shaft in order to measure accurate values of applied torque by sensing the actual shaft deflection caused by a twisting force. The snapshot and the frame assignments of MyBot arm are shown in Fig. 2. Note that the base frame $\{0\}$ is located at the screen. In the proposed calibration system, there exist four sources of errors:

- small errors existing in the geometric parameter,
- small errors existing in the laser module (LM),
- encoder errors existing in each joint coordinate, and
- measurement errors existing in the stationary camera.

The geometric parameter errors can be represented by deriving the kinematic equations of MyBot arm using the D-H method. Since the base frame $\{0\}$ is located at the screen, the transformation matrix between frame $\{0\}$ and $\{1\}$ involves five parameters as follows:

$$
\begin{aligned}
{}^{0}_{1}\mathbf{T} &= \mathbf{T}_{tx} \cdot \mathbf{T}_{tz} \cdot \mathbf{T}_{rx} \cdot \mathbf{T}_{ry} \cdot \mathbf{T}_{rz} \cdot \mathbf{T}_{q} \\
&= \mathrm{trans}(x, a_1 + \delta k_1) \cdot \mathrm{trans}(z, d_1 + \delta k_2) \cdot \mathrm{rot}(x, \alpha_1 + \delta k_3) \\
&\cdot \mathrm{rot}(y, \beta_1 + \delta k_4) \cdot \mathrm{rot}(z, \theta_1 + \delta k_5) \cdot \mathrm{rot}(z, q_1) \qquad (1)
\end{aligned}
$$

where trans and rot correspond to translation and rotation, respectively. q is the value of joint coordinate and δk represents the physical error existing in the geometric parameter. The nominal values of D-H parameters are summarized in Table I.

The mutual perpendicular axes always exist between two consecutive joints from frame $\{1\}$ to $\{7\}$ because the MyBot arm is made up of seven revolute joints. In other words, there are no translation and rotation components along the y-axis between two revolute joints. Thus, each transformation matrix from frame $\{1\}$ to $\{7\}$ consists of four D-H parameters as follows:

$$
\begin{aligned}
{}^{i-1}_{i}\mathbf{T} &= \mathbf{T}_{tx} \cdot \mathbf{T}_{tz} \cdot \mathbf{T}_{rx} \cdot \mathbf{T}_{rz} \cdot \mathbf{T}_{q} \\
&= \mathrm{trans}(x, a_i + \delta k_{4i-2}) \cdot \mathrm{trans}(z, d_i + \delta k_{4i-1}) \cdot \\
&\mathrm{rot}(x, \alpha_i + \delta k_{4i}) \cdot \mathrm{rot}(z, \theta_i + \delta k_{4i+1}) \cdot \mathrm{rot}(z, q_i) \qquad (2)
\end{aligned}
$$

where $i = 2, \ldots, 7$.

The last transformation matrix between frame $\{7\}$ to $\{\mathrm{LM}\}$ is made up of six parameters: three translations and

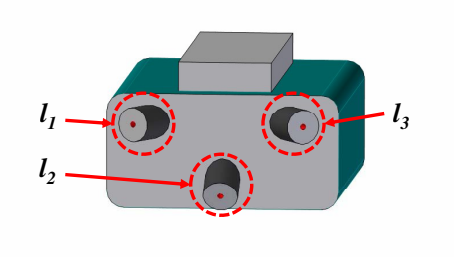

Fig. 3. Laser module having three laser sources (l_1, l_2, and l_3).

three rotations. However, the translation error along the direction of laser source cannot be measured. Note that this translation error does not affect any variation on the measurement on the 2D screen as well. Thus, the transformation matrix between frame {7} and {LM} involves five parameters as follows:

$$\begin{aligned} {}^{7}_{LM}\mathbf{T} &= \mathbf{T}_{tx} \cdot \mathbf{T}_{tz} \cdot \mathbf{T}_{rx} \cdot \mathbf{T}_{ry} \cdot \mathbf{T}_{rz} \\ &= \text{trans}(x, a_{LM} + \delta k_{30}) \cdot \text{trans}(z, d_{LM} + \delta k_{31}) \cdot \\ &\text{rot}(x, \alpha_{LM} + \delta k_{32}) \cdot \text{rot}(y, \beta_{LM} + \delta k_{33}) \cdot \text{rot}(z, \theta_{LM} + \delta k_{34}). \end{aligned} \tag{3}$$

According to [2], the correct numbers of geometric parameters for completeness are $4R$ + $2P$ + 6, where R and P represent the number of revolute and prismatic joints, respectively. Since $R = 7$ and $P = 0$ in our case, the number of geometric parameters for completeness becomes 34, which is equivalent to $\delta\mathbf{k} = \{\delta k_1, \ldots, \delta k_{34}\}$.

The laser module made with three laser sources is attached to the end-effector of the MyBot arm, which is used to measure an accurate position of the end-effector. Fig. 3 shows the image of the laser module, where three transformation matrices from the laser module to each laser source, l_1, l_2, and l_3, are defined as follows:

$$\begin{aligned} {}^{LM}_{l_1}\mathbf{T} &= \text{rot}\,(x, -30.0^\circ) \\ {}^{LM}_{l_2}\mathbf{T} &= \text{rot}\,(y, -30.0^\circ) \\ {}^{LM}_{l_3}\mathbf{T} &= \text{rot}\,(x, 30.0^\circ)\,. \end{aligned} \tag{4}$$

As stated above, the second source of errors is the physical offset errors existing in the laser module during the manufacturing process. However, these error values must be calibrated separately before attaching to the end-effector of the manipulator.

Based on the above information, three kinematic equations that represent the relationship between the base frame and each of three laser sources can be calculated by multiplying the individual link-transformation matrices together as follows:

$${}^{0}_{l_j}\mathbf{T} = \left(\prod_{i=1}^{7} {}^{i-1}_{i}\mathbf{T}\right) \cdot {}^{7}_{LM}\mathbf{T} \cdot {}^{LM}_{l_j}\mathbf{T} = \begin{bmatrix} \mathbf{x} & \mathbf{y} & \mathbf{z} & \mathbf{p} \\ 0 & 0 & 0 & 1 \end{bmatrix} \tag{5}$$

where $j = 1, 2, 3$. The third source of errors is the encoder error existing in each joint coordinate, $\mathbf{q} = \{q_1, \ldots, q_7\}$. DC motors and harmonic drives of the MyBot arm are directly connected to each other, which provides a resolution of 0.0009° per step. Thus, the geometric parameter errors are only considered in the calibration model.

The last source of errors is the measurement error existing in the stationary camera. Due to the lens distortion, captured images from the stationary camera must be corrected to measure the accurate positions of laser beams on the 2D screen. Random measurement noise is added in the simulation to account for the measurement error model.

III. Jacobian Matrices Formulation

In order to estimate accurate geometric parameter errors of kinematic equations, two Jacobian matrices are derived in this section. Differential kinematic is used to derive the first Jacobian matrix, which relates the velocities of geometric parameters and the motion of end-effector. Then the general transformation mapping is used to obtain the second Jacobian matrix that relates the motion of end-effector and the positions of laser beams on the screen. When these two matrices are multiplied, a non-singular Jacobian matrix is formulated, which represents the relationship between 34 geometric parameter errors of MyBot arm and the positions of three laser beams on the 2D screen.

The concept of differential motion is applied to derive the first Jacobian matrix because small differential motion causes the errors between the theoretical and the measured positions [13]. Transformation matrix between frame {1} to frame {l} can be expressed as a 6×5 matrix as follows:

$$\begin{bmatrix} {}^{l}\partial v_x \\ {}^{l}\partial v_y \\ {}^{l}\partial v_z \\ {}^{l}\partial w_x \\ {}^{l}\partial w_y \\ {}^{l}\partial w_z \end{bmatrix} = {}^{1}\mathbf{J}(\Delta) \begin{bmatrix} {}^{1}\partial v_x \\ {}^{1}\partial v_z \\ {}^{1}\partial w_x \\ {}^{l}\partial w_y \\ {}^{1}\partial w_z \end{bmatrix} \tag{6}$$

with

$${}^{1}\mathbf{J}(\Delta) = \begin{bmatrix} \mathbf{x}_{tx} & \mathbf{z}_{tz} & \mathbf{x}_{rx} \times {}^{1}\mathbf{p}_l & \mathbf{y}_{ry} \times {}^{1}\mathbf{p}_l & \mathbf{z}_{rz} \times {}^{1}\mathbf{p}_l \\ 0_{3\times1} & 0_{3\times1} & \mathbf{x}_{rx} & \mathbf{y}_{ry} & \mathbf{z}_{rz} \end{bmatrix}$$

where v and w represent the linear and rotational velocities, respectively. The value of each component can be directly found by using the transformation matrix ${}^{0}_{1}\mathbf{T}$, where the value of ${}^{1}\mathbf{p}_l$ equals the difference between ${}^{0}\mathbf{p}_1$ and ${}^{0}\mathbf{p}_l$. Note that the order of linear and rotational velocities in (6) is equivalent to the order of the derivative of D-H parameters in (1).

In this manner, Jacobian matrix that relates the motion of individual joints to end-effector denoted as, $\mathbf{Jac}_1$, can be defined as follows:

$$\mathbf{Jac}_1 = \begin{bmatrix} {}^{1}\mathbf{J}(\Delta) & {}^{2}\mathbf{J}(\Delta) \cdots {}^{7}\mathbf{J}(\Delta) & {}^{LM}\mathbf{J}(\Delta) \end{bmatrix} \tag{7}$$

where the size of $\mathbf{Jac}_1$ is 6×34.

The general transformation mapping is employed to derive the second Jacobian matrix. Position and velocity vectors of the laser source attached on the laser module between the base frame and the end-effector frame can be represented as

follows:

$$
\begin{aligned}
{}^0\mathbf{p}_l &= {}^l\mathbf{p}_l + {}^0_l\mathbf{R}\begin{bmatrix}0\\0\\1\end{bmatrix}k \\
{}^0\dot{\mathbf{p}}_l &= {}^l\dot{\mathbf{p}}_l + \begin{bmatrix}w_x\\w_y\\w_z\end{bmatrix}\times\left({}^0_l\mathbf{R}\begin{bmatrix}0\\0\\1\end{bmatrix}k\right) + {}^0_l\mathbf{R}\begin{bmatrix}0\\0\\1\end{bmatrix}\dot{k} \quad (8)
\end{aligned}
$$

where ${}^0_l\mathbf{R}$ describes the rotation matrix in frame $\{l\}$ relative to frame $\{0\}$, k and $\dot{k}$ represent the distance and the speed between the laser source and the laser beam on screen, respectively. Since the screen is equivalent to the base frame $\{0\}$ as shown in Fig. 1, x-component of the position vector, ${}^0\mathbf{p}_l$, becomes zero and the value of k can be calculated as follows:

$$
\begin{aligned}
{}^0\mathrm{p}_x &= {}^l\mathrm{p}_x + \mathrm{z}_x k = 0 \\
k &= -\frac{{}^l\mathrm{p}_x}{\mathrm{z}_x}. \quad (9)
\end{aligned}
$$

Similarly, x-component of the velocity vector, ${}^0\dot{\mathbf{p}}_l$, is also zero and the value of $\dot{k}$ can be calculated by substituting (9) into (8) as follows:

$$
\begin{aligned}
{}^0\dot{\mathrm{p}}_x &= {}^l\dot{\mathrm{p}}_x + (w_y\mathrm{z}_z - w_z\mathrm{z}_y)k + \mathrm{z}_x\dot{k} = 0 \\
\dot{k} &= -\frac{{}^l\dot{\mathrm{p}}_x\mathrm{z}_x - (w_y\mathrm{z}_z - w_z\mathrm{z}_y){}^l\mathrm{p}_x}{\mathrm{z}_x^2}. \quad (10)
\end{aligned}
$$

In this manner, two equations that relate the end-effector velocities to the laser velocities on the screen are given by expanding the velocity vector of (8) as follows:

$$
\begin{aligned}
{}^0\dot{\mathrm{p}}_y &= {}^l\dot{\mathrm{p}}_y + (w_z\mathrm{z}_x - w_x\mathrm{z}_z)k + \mathrm{z}_y\dot{k} = 0 \\
{}^0\dot{\mathrm{p}}_z &= {}^l\dot{\mathrm{p}}_z + (w_x\mathrm{z}_y - w_y\mathrm{z}_x)k + \mathrm{z}_z\dot{k} = 0. \quad (11)
\end{aligned}
$$

Substituting (9) and (10) into (11), we obtain

$$
\begin{bmatrix}{}^0\partial v_y\\{}^0\partial v_z\end{bmatrix} = \mathbf{Jac}_2\begin{bmatrix}{}^l\partial v_x\\{}^l\partial v_y\\{}^l\partial v_z\\{}^l\partial w_x\\{}^l\partial w_y\\{}^l\partial w_z\end{bmatrix} \quad (12)
$$

with

$$
\mathbf{Jac}_2 = \begin{bmatrix}
-\frac{\mathrm{z}_y}{\mathrm{z}_x} & 1 & 0 & \frac{\mathrm{z}_z{}^l\mathrm{p}_x}{\mathrm{z}_x} & \frac{\mathrm{z}_z\mathrm{z}_y{}^l\mathrm{p}_x}{\mathrm{z}_x^2} & -\frac{\left(1-\mathrm{z}_z^2\right){}^l\mathrm{p}_x}{\mathrm{z}_x^2} \\
-\frac{\mathrm{z}_z}{\mathrm{z}_x} & 0 & 1 & -\frac{\mathrm{z}_y{}^l\mathrm{p}_x}{\mathrm{z}_x} & \frac{\left(1-\mathrm{z}_y^2\right){}^l\mathrm{p}_x}{\mathrm{z}_x^2} & -\frac{\mathrm{z}_z\mathrm{z}_y{}^l\mathrm{p}_x}{\mathrm{z}_x^2}
\end{bmatrix}
$$

where this 2×6 matrix is denoted as $\mathbf{Jac}_2$, which represents the Jacobian matrix that relates the end-effector velocities to the laser velocities on the screen.

A non-singular Jacobian matrix, $\mathbf{J}$, that relates the velocities of 34 geometric parameter errors and the laser beam velocities on the screen for three laser sources - l_1, l_2, and l_3 - can be formulated by multiplying $\mathbf{Jac}_1$ and $\mathbf{Jac}_2$ as follows:

$$
\mathbf{J} = \begin{bmatrix}{}^{l_1}\mathbf{Jac}_2{}^{l_1}\mathbf{Jac}_1\\{}^{l_2}\mathbf{Jac}_2{}^{l_2}\mathbf{Jac}_1\\{}^{l_3}\mathbf{Jac}_2{}^{l_3}\mathbf{Jac}_1\end{bmatrix} \quad (13)
$$

where the size of $\mathbf{J}$ is 6×34. This Jacobian matrix will be utilized in parameter estimation algorithms presented in the following section.

IV. Parameter Estimation Algorithm

Two parameter estimation algorithms, LSE and EKF, are employed to estimate the accurate value of geometric parameter errors. Initially, the position of three laser beams for n number of poses chosen over the whole manipulator workspace should be obtained by the stationary camera. Then the position error vector, $\mathbf{e}$, can be calculated by the difference between the measured position and the theoretical position from (8).

The parameter updating procedure of LSE is given as follows:

$$
\delta\hat{\mathbf{k}}_{t+1} = (\tilde{\mathbf{J}}_t^T\tilde{\mathbf{J}}_t)^{-1}\tilde{\mathbf{J}}_t^T\tilde{\mathbf{e}}_t + \delta\hat{\mathbf{k}}_t \quad (14)
$$

where

$$
\tilde{\mathbf{e}} = \begin{bmatrix}\mathbf{e}^{(1)}\\\mathbf{e}^{(2)}\\\vdots\\\mathbf{e}^{(n)}\end{bmatrix}, \quad \tilde{\mathbf{J}} = \begin{bmatrix}\mathbf{J}^{(1)}\\\mathbf{J}^{(2)}\\\vdots\\\mathbf{J}^{(n)}\end{bmatrix}. \quad (15)
$$

Note that the size of $\tilde{\mathbf{e}}$ and $\tilde{\mathbf{J}}$ are $6n \times 1$ and $6n \times 34$, respectively.

The parameter updating procedure of EKF is given as follows:

$$
\delta\hat{\mathbf{k}}_{t+1} = \{\mathbf{P}_t\tilde{\mathbf{J}}_t^T(\tilde{\mathbf{J}}_t\mathbf{P}_t\tilde{\mathbf{J}}_t^T + \mathbf{R})^{-1}\}\tilde{\mathbf{e}}_t + \delta\hat{\mathbf{k}}_t \quad (16)
$$

and

$$
\mathbf{P}_{t+1} = \{\mathbf{I} - \mathbf{P}_t\tilde{\mathbf{J}}_t^T(\tilde{\mathbf{J}}_t\mathbf{P}_t\tilde{\mathbf{J}}_t^T + \mathbf{R})^{-1}\tilde{\mathbf{J}}_t\}\mathbf{P}_t + \mathbf{Q} \quad (17)
$$

where $\mathbf{I}$ is the identity matrix, $\mathbf{Q}$ and $\mathbf{R}$ are the covariance matrices of system noise and measurement noise, respectively. Note that if $\mathbf{Q}$ and $\mathbf{R}$ are set to zero, then EKF simply reduces to Newton-Raphson method.

Once the updating procedure is completed, norm values of parameter vector and position error vector are calculated for every iteration. The updating procedure is iterated until these norm values converge to certain desired values, which are defined by user.

V. Simulation Results

To verify the effectiveness of the proposed technique, the error values of all geometric parameters were set as (δa, δd, $\delta\alpha$, $\delta\beta$, $\delta\theta$) = (10.0 mm, 10.0 mm, 1.0°, 1.0°, 1.0°) in the simulation. The maximum number of iteration for both LSE and EKF was set as $10,000$, where the iteration terminated when the norm value of parameter vector and position error vector were less than 1.0×10^{-7}. For EKF, both $\mathbf{Q}$ and $\mathbf{R}$ were set as $1.0 \times 10^{-4}\mathbf{I}_{34}$.

TABLE II

DISTANCE ERRORS OF THREE LASER BEAMS ON THE SCREEN BEFORE CALIBRATION.

	Calibration Set (mm)									
		l_1			l_2			l_3		
	Poses	Mean	STD	Max	Mean	STD	Max	Mean	STD	Max
Case 1	10	84.1	10.2	99.1	322.0	148.6	629.7	183.6	51.6	307.0
Case 2	30	83.8	9.2	101.0	317.1	131.1	646.3	190.1	55.9	314.3
Case 3	50	83.5	9.9	102.9	322.9	143.2	831.1	187.7	60.6	413.5
Case 4	70	82.2	10.1	102.9	339.9	153.8	831.1	191.5	61.5	413.5
Case 5	100	82.8	10.2	109.2	340.8	147.0	831.1	191.3	57.6	413.5
Case 6	150	82.4	10.4	109.2	337.0	157.3	898.9	190.0	57.6	413.5
	Testing Set (mm)									
		l_1			l_2			l_3		
	Poses	Mean	STD	Max	Mean	STD	Max	Mean	STD	Max
Case 1	140	82.3	10.4	109.2	338.1	157.9	898.9	190.5	58.0	413.5
Case 2	120	82.0	10.7	109.2	342.0	162.8	898.9	190.0	58.0	413.5
Case 3	100	81.8	10.6	109.2	344.1	163.4	898.9	191.2	56.0	389.5
Case 4	80	82.6	10.7	109.2	334.5	160.3	898.9	188.8	54.0	389.5
Case 5	50	81.6	10.8	104.7	329.5	175.9	898.9	187.5	57.6	389.5

TABLE III

COMPARISON BETWEEN TWO ALGORITHMS WITHOUT ADDING MEASUREMENT NOISE.

		LSE		EKF	
	Poses	Iteration	Time	Iteration	Time
Case 1	10	6	0.5”	3,359	3’18”
Case 2	30	5	0.8”	1,236	3’18”
Case 3	50	5	1.2”	866	3’28”
Case 4	70	6	1.8”	701	3’35”
Case 5	100	5	1.9”	570	3’58”
Case 6	150	5	2.4”	381	3’59”

A total of 150 poses were randomly generated over the whole MyBot arm workspace shown in Table I and then the positions of three laser beams on the screen for each poses were measured. Among 150 generated poses, it was divided into six cases, which were composed of calibration and testing set as follows:

- Case 1: 10 calibration poses, 140 testing poses
- Case 2: 30 calibration poses, 120 testing poses
- Case 3: 50 calibration poses, 100 testing poses
- Case 4: 70 calibration poses, 80 testing poses
- Case 5: 100 calibration poses, 50 testing poses
- Case 6: 150 calibration poses.

The calibration set was used as an input to the parameter estimation algorithms, where the testing set was used to verify the estimated geometric parameter errors. The proposed algorithm was evaluated by calculating a distance error between the measured position of laser beams on the screen and the theoretical position obtained by using (8). Table II shows the distance error for all six cases before the calibration procedure, which includes the mean distance error, the standard deviation, and the maximum distance error.

Table III summarizes the number of converged iteration and the corresponding run time measured from MATLAB when the measurement noise was not added. The results showed that LSE converged significantly faster than EKF. Note that the norm value of 34 parameters for EKF was less than 0.01 within 10 iterations as well. Since both algorithms perfectly estimated the predefined error value of geometric parameters, the distance errors of the calibration and the testing set for all six cases were zero. For EKF, the number of converged iteration was decreased as the number of calibration poses was increased. In contrast, the run time was increased because the time to calculate the inverse matrix in (16) was increased.

When the positions of three laser beams on the screen were measured, a random noise of $[-2.0$ mm, 2.0 mm$]$ was added to cope with the measurement error existing in the stationary camera. Table IV presents the distance error of all six cases after the calibration procedure by using LSE and EKF. When the estimated geometric parameter vector, $\mathbf{k}$, was added to the nominal values shown in Table I, the accuracy was improved as the number of calibration pose increases. The results of the calibration set showed that EKF performed better than LSE because the mean error values of three laser beams for EKF were less than 1.0 mm for all six cases. In contrast, these values for LSE were less than 1.0 mm when the calibration set was made up of more than 50 poses.

Fig. 4 shows the accuracy of testing sets from Table IV for better visibility. The results of the testing set also showed that EKF performed better than LSE. When 10 calibration poses were used, the mean error value of EKF was lowered than the mean value of LSE by a factor of 4.4. This value was decreased by a factor of 6.9 when the number of calibration poses was increased to 30. However, the mean distance errors between the measured positions and the theoretical positions for both LSE and EKF were less than 0.4 mm when the calibration poses were greater than 50.

The simulation results confirmed that the proposed technique allowed to estimate the entire geometric parameter errors with the small number of measurements when the EKF was used as a parameter estimation algorithm. Without measurement noise, LSE converged faster than EKF. However, LSE required more number of measurements compared to EKF when the measurement noise was considered in the kinematic model. In order to move the end-effector in a specified direction at a specified speed with accuracy, the motion of individual joints must be coordinated. In this paper, the differential relationship between joint displacements and laser module was represented as a non-singular Jacobian matrix, and then the variances between actual and measured laser positions that influence the direction and speed of laser module were formulated to estimate entire and accurate geometric parameters of manipulator.

VI. CONCLUSIONS

This paper proposed the kinematic calibration technique by utilizing the laser module and the stationary camera.

TABLE IV

DISTANCE ERRORS OF THREE LASER BEAMS ON THE SCREEN AFTER CALIBRATION USING LSE AND EKF.

	Calibration Set (mm)																		
	Poses	LSE									EKF								
		l_1			l_2			l_3			l_1			l_2			l_3		
		Mean	STD	Max	Mean	STD	Max	Mean	STD	Max	Mean	STD	Max	Mean	STD	Max	Mean	STD	Max
Case 1	10	1.02	0.37	1.60	2.37	0.81	3.88	1.02	0.33	1.53	**0.34**	0.10	0.49	**0.36**	0.18	0.59	**0.27**	0.09	0.48
Case 2	30	0.83	0.24	1.20	2.26	0.85	4.53	0.76	0.18	1.15	**0.16**	0.07	0.33	**0.26**	0.16	0.59	**0.17**	0.07	0.29
Case 3	50	0.20	0.10	0.51	**0.25**	0.17	0.87	0.23	0.14	0.71	**0.13**	0.07	0.28	0.27	0.13	0.65	**0.15**	0.10	0.49
Case 4	70	0.15	0.07	0.33	0.34	0.15	0.64	0.18	0.10	0.39	**0.14**	0.08	0.33	**0.21**	0.13	0.55	**0.11**	0.06	0.33
Case 5	100	0.15	0.09	0.49	0.21	0.12	0.77	0.17	0.11	0.51	**0.10**	0.06	0.24	**0.20**	0.12	0.56	**0.09**	0.05	0.25
Case 6	150	0.16	0.09	0.48	0.39	0.27	1.51	0.14	0.08	0.47	**0.08**	0.04	0.20	**0.15**	0.08	0.53	**0.07**	0.05	0.27
	Testing Set (mm)																		
	Poses	LSE									EKF								
		l_1			l_2			l_3			l_1			l_2			l_3		
		Mean	STD	Max	Mean	STD	Max	Mean	STD	Max	Mean	STD	Max	Mean	STD	Max	Mean	STD	Max
Case 1	140	1.15	0.51	2.44	2.74	1.69	13.78	1.38	0.85	5.95	**0.35**	0.14	0.77	**0.56**	0.38	2.54	**0.28**	0.17	0.96
Case 2	120	0.92	0.29	1.62	2.73	1.35	8.75	0.85	0.22	1.42	**0.16**	0.08	0.49	**0.34**	0.27	1.83	**0.16**	0.07	0.33
Case 3	100	0.24	0.11	0.57	**0.25**	0.15	0.91	0.25	0.14	0.76	**0.14**	0.07	0.34	0.26	0.14	0.67	**0.16**	0.09	0.39
Case 4	80	0.19	0.11	0.60	0.39	0.21	1.54	0.20	0.10	0.50	**0.15**	0.07	0.36	**0.21**	0.12	0.51	**0.10**	0.05	0.26
Case 5	50	0.15	0.09	0.36	**0.23**	0.16	0.97	0.16	0.10	0.37	**0.11**	0.05	0.21	**0.23**	0.14	0.64	**0.09**	0.06	0.31

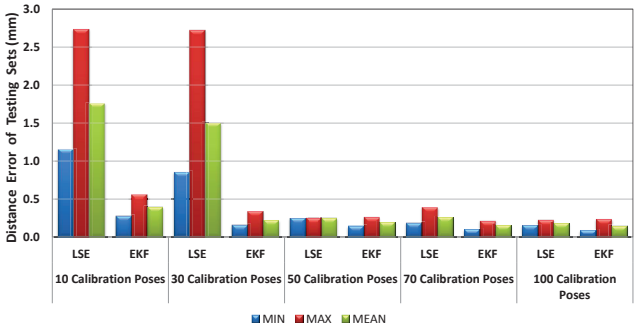

Fig. 4. Accuracy of the MyBot arm after calibration.

The proposed technique was able to estimate entire geometric parameter errors by formulating the non-singular Jacobian matrix between each geometric parameters and the actual measurements. Significantly, this Jacobian matrix considered both position and orientation information of all joint coordinates and the end-effector. Simulation results confirmed that both LSE and EKF successfully estimated the predefined parameter errors. However, EKF converged with a small number of measurements compared to LSE when the measurement noise was added. Verifying the proposed technique in real experiment is left as a future work.

ACKNOWLEDGMENTS

This research was supported by Basic Science Research Program through the National Research Foundation of Korea (NRF) funded by the Ministry of Education, Science and Technology (2011-0000321).

REFERENCES

[1] Z. Roth, B. Mooring and B. Ravani, "An overview of robot calibration," *IEEE J. Robotics and Automation*, vol. 3, no. 5, pp. 377–385, 1987.

[2] B. Mooring, Z. Roth and M. Driels, *Fundamentals of Manipulator Calibration*. New York: Wiley, 1991.

[3] Z. Zhuang and Z. Roth, *Camera-Aided Robot Calibration*. Boca Raton, FL: CRC Press, 1996.

[4] J. Hollerbach and C. Wampler, "The calibration index and taxonomy for robot kinematic calibration methods," *The Int. J. Robotics Research*, vol. 15, pp. 573–591, 1996.

[5] A. Omodei, G. Legnani and R. Adamini, "Three methodologies for the calibration of industrial manipulators: experimental results on a SCARA robot," *J. Robotic Systems*, vol. 17, no. 6, pp. 291–307, 2000.

[6] G. Alici and B. Shirinzadeh, "A systematic technique to estimate positioning errors for robot accuracy improvement using laser interferometry based sensing," *Mechanism and Machine Theory*, vol. 40, pp. 879–906, 2005.

[7] P. Renaud, N. Andreff, J.-H. Lavest and M. Dhome, "Simplifying the kinematic calibration of parallel mechanisms using vision-based metrology," *IEEE Trans. Robotics*, vol. 22, no. 1, pp. 12–22, 2006.

[8] A. Omodei, G. Legnani and R. Adamini, "Calibration of a measuring robot: experimental results on a 5 DOF structure," *J. Robotic Systems*, vol. 18, no. 5, pp. 237–250, 2001.

[9] G. Gatti and G. Danieli, "A practical approach to compensate for geometric errors in measuring arms: application to a six-degree-of-freedom kinematic structure," *Meas. Sci. and Technol.*, vol. 19, no. 1, pp. 015107-10015107-12, 2008.

[10] J. Santolaria, J. Aguilar, J. Yague and J. Pastor, "Kinematic parameter estimation technique for calibration and repeatability improvement of articulated arm coordinate measuring machines," *Precision Engineering*, vol. 32, pp. 251–268, 2008.

[11] C. C. Iurascu and F. C. Park, "Geometric algorithms for kinematic calibration of robots containing closed loops," *J. Mechanical Design*, vol. 125, pp. 23–32, 2003.

[12] S. Ye, Y. Wang, Y. Ren and D. Li, "Robot calibration using iteration and differential kinematics," *J. Physics: Conference Series*, vol. 48, pp. 1–6, 2006.

[13] P. J. McKerrow, *Introduction to Robotics*. Sydney, Australia: Addison-Wesley, 1991.